Advances in Nano Research, *Vol. 12, No. 5 (2022) 441-455*
https://doi.org/10.12989/anr.2022.12.5.441

Nonlinear bending analysis of porous sigmoid FGM nanoplate via IGA and nonlocal strain gradient theory

Thanh Cuong-Le*[1], Khuong D. Nguyen[2,3], Hoang Le-Minh[1], Phuong Phan-Vu[1], Phuoc Nguyen-Trong[1], Abdelouahed Tounsi[4,5,6]

[1]*Faculty of Civil Engineering, Ho Chi Minh City Open University, Ho Chi Minh City, Vietnam*
[2]*Department of Engineering Mechanics, Faculty of Applied Science, Ho Chi Minh City University of Technology (HCMUT), Ho Chi Minh City, Vietnam*
[3]*Vietnam National University, Ho Chi Minh City, Vietnam*
[4]*YFL (Yonsei Frontier Lab), Yonsei University, Seoul, Korea*
[5]*Department of Civil and Environmental Engineering, King Fahd University of Petroleum & Minerals, 31261 Dhahran, Eastern Province, Saudi Arabia.*
[6]*Material and Hydrology Laboratory, University of Sidi Bel Abbes, Faculty of Technology, Civil Engineering Department, Algeria*

(*Received September 26, 2021, Revised February 2, 2022, Accepted February 4, 2022*)

Abstract. This study explores the linear and nonlinear solutions of sigmoid functionally graded material (S-FGM) nanoplate with porous effects. A size-dependent numerical solution is established using the strain gradient theory and isogeometric finite element formulation. The nonlinear nonlocal strain gradient is developed based on the Reissner-Mindlin plate theory and the Von-Kármán strain assumption. The sigmoid function is utilized to modify the classical functionally graded material to ensure the constituent volume distribution. Two different patterns of porosity distribution are investigated, viz. pattern A and pattern B, in which the porosities are symmetric and asymmetric varied across the plate's thickness, respectively. The nonlinear finite element governing equations are established for bending analysis of S-FGM nanoplates, and the Newton-Raphson iteration technique is derived from the nonlinear responses. The isogeometric finite element method is the most suitable numerical method because it can satisfy a higher-order derivative requirement of the nonlocal strain gradient theory. Several numerical results are presented to investigate the influences of porosity distributions, power indexes, aspect ratios, nonlocal and strain gradient parameters on the porous S-FGM nanoplate's linear and nonlinear bending responses.
Keywords: isogeometric analysis; nonlinear bending; nonlocal strain gradient; porosity; S-FGM nanoplate

1. Introduction

The functionally graded material (FGM) plays a primary class of advanced composite materials. By the combination of two or more different materials, the FGM produces better physical-mechanical properties. The classical FGM was firstly introduced by Koizum (1993). Since then, FGM has worldwide applications in many fields, such as sensors, biomaterial, dental implants, automobiles, aerospace, nuclear energy (Miyamoto *et al*. 2013, Pompe 2003, Mueller *et al*. 2003). The power-law and Mori-Tanaka scheme are assumed commonly to define the material properties of FGM. However, the stress assembles in one of the interfaces, wherein the material is rapidly changing. Consequently, the sigmoid function is utilized to get two-volume fractions across the plate's thickness, and the stress can obtain the smooth variation through the thickness of the plate (Chung and Chi 2001).

The experimental data has proved that the mechanical properties of micro/nanostructures refer to the small size effect in many engineering fields of real-life application. For instance, the thin film, nanographene sheet, carbon nanotube, functionally graded, and sandwich plate have broad applications in micro/nano-electromechanical devices, biological implant, sensor, and aerospace (He *et al*. 2018, Gain *et al*. 2016, Xiang *et al*. 2020, Moory-Shirbani *et al*. 2018). Therefore, the higher-order continuum theories have been developed to reach the accurate analysis of the responses of these types of structures, such as Eringen's nonlocal theory (Eringen 1972a, b), couple stress theory (Toupin 1962, Koiter 1964), strain gradient theory (Mindlin 1963, Mindlin 1968), modified couple stress theory (Yang *et al*. 2002).

Over the past few years, researchers have been attracted to investigate the mechanical response of micro/nanoplates. Through the numerical models and experimental studies, Eringen's nonlocal elasticity theory has been proved its accuracy in predicting the mechanical responses of nanoplate. A nonlocal analytical solution for static bending, free vibration, buckling, and thermal buckling of FGM nanoplate bearing on an elastic foundation was presented by Sobhy (2015). Mechab *et al*. (2016) provided a Navier analytical solution for free vibration responses of FGM nanoplate resting on elastic foundation using nonlocal higher-order shear deformation theory with the refined distributed shape function. Ansari *et al*. (2018) presented the finite element nonlocal theory for static bending of nanoplate bearing on an elastic foundation. Ma *et al*. (2018)

*Corresponding author, Ph.D.,
E-mail: cuong.lt@ou.edu.vn

ISSN: 2287-237X (Print), 2287-2388 (Online)

performed the wave propagation of piezoelectric nanoplate using nonlocal theory, Mindlin and Kirchhoff plate theories. Ebrahimi and Barati (2019) carried out the free vibration of the flexoelectric nanoplate embedded the Winkler and Pasternak foundations. Karami and Kanami (2019) adopted the nonlocal strain gradient theory and the refined plate theory to obtain the buckling responses of FGM nanoplate in a thermal environment. Fattahi *et al*. (2019) applied the Reddy higher-order plate theory and nonlocal theory to investigate the free vibration of the FGM nanoplate resting on the Pasternak foundation. Arefi *et al*. (2018) studied free vibration of FG porosity sandwich nanoplate with piezomagnetic face layers bearing on Pasternak foundation based on nonlocal strain gradient theory. Singh and Azam (2020) utilized the Rayleigh-Ritz method to derive the buckling and free vibration behaviours of the FGM nanoplate resting on the Winkler–Pasternak foundation using the nonlocal elastic theory. Liu *et al*. (2021) established the nonlocal strain gradient governing equations to investigate the vibration response of laminated nanoplates with piezo-magnetic face layers. Emadi *et al*. (2021) explored the small size influence on buckling responses of bi-directional FGM nanoplate. Numerical and analytical solutions have been established to explore the mechanical response of structures (Ouakad *et al*. 2020, Shariati *et al*. 2020a, Sedighi *et al*. 2020, Sedighi and Malikan 2020, Koochi and Goharimanesh 2021, Abouelregal *et al*. 2021, Zhou *et al*. 2020, Yan *et al*. 2020, She *et al*. 2020, Faled *et al*. 2018, Khalaf *et al*. 2019, Si *et al*. 2020, Khaniki *et al*. 2020, Abdulrazzaq *et al*. 2020, Shan *et al*. 2020, Khazaei and Mahammadimehr 2020, Ebrahimi and Seyfi 2020, Ebrahimi *et al*. 2021, Sahmani *et al*. 2020, Wang 2018, Wang and Zu 2017a, Ye and Wang 2021).

More recently, studying the mechanical responses of the S-FGM has been attractive to researchers. Kaci *et al*. (2013) presented the nonlinear bending of the S-FGM plate. Lee *et al*. (2015) established an analytical solution for bending behaviours of a simply-supported S-FGM plate subjected elastic foundation sing a refined plate theory. Thang *et al*. (2016) presented a nonlinear closed-form solution for nonlinear responses of the S-FGM plate bearing on the elastic medium. Wang and Zu (2017b) investigated the influence of porosity on the large-amplitude vibration of S-FGM. Singh and Harsha (2019) presented the nonlinear free vibration of the S-FGM sandwich plate bearing on the Pasternak foundation. Singh and Harsha (2020) also investigated porous S-FGM sandwich plates' dynamic and buckling responses embedded in the Pasternak foundation. However, very few solutions have been developed for S-FGM nanoplate based on higher-order continuum elastic theories. Kim *et al*. (2014) explored the free vibration of the S-FGM nanoplate using the nonlocal elastic theory. Daikh *et al*. (2021) presented an analytical nonlocal strain gradient model to study the bending responses of the S-FGM sandwich nanoplate. Van Vinh (2022) adopted a nonlocal elastic theory to explore the free vibration responses of the S-FGM nanoplate. Also, some porous and nanostructures models (Ahmed *et al*. 2020, Shariati *et al*. 2020b, Ebrahimi *et al*. 2020, Fenjan *et al*. 2020a, b, Teng and Wang 2021, Xu *et al*. 2021, Wang and Zu 2019, Chai and Wang 2022, Ishihara *et al*. 2020) were established.

The developed numerical nanoplate models based on the higher-order continuum theory generate the higher-order derivative terms. Therefore, isogeometric analysis (IGA) (2005) has been proved as a robust method to derive the responses of micro/nanoplates due to higher-order continuity between two elements. A NURBS geometry is built by the NURBS basic functions used in the finite discretization process. IGA has been demonstrated as an effective computational method by using higher-order basic functions because it can produce ultra-convergence and high accuracy numerical solutions in the literature. Natarajan *et al*. (2012) studied free vibration of FG nanoplate using IGA and nonlocal elasticity theory. Fan *et al*. (2021) investigated the buckling and post-buckling responses of porous FG micro/nanoplates based on IGA and the nonlocal strain gradient theory. Norouzzadeh *et al*. (2019) established a size-dependent IGA Timoshenko solution to explore the nonlinear static bending of isotropic nanobeam. Ansari and Norouzzadeh (2016) proposed an IGA nonlocal model to study the buckling behaviours of FG nanoplate with skew, circular and elliptical geometry. The small size-dependent of micro/nanoplates have been derived by using the NURBS-based finite element such as Chen *et al*. (2019), Liu *et al*. (2020), Thanh *et al*. (2019a, b, 2020, 2021), Thai *et al*. (2021), Rabczuk *et al*. (2019), Samaniego *et al*. (2020), Zhuang *et al*. (2021).

This article aims to establish a small size-dependent isogeometric analysis finite element model based on the nonlocal strain gradient theory to investigate the linear and nonlinear responses of the porous S-FGM nanoplate. The asymmetric and asymmetric porosity distribution patterns are utilized to investigate the porosity effect on nonlinear bending responses. Reissner-Mindlin plate theory, the nonlocal strain gradient theory, and the Von-Kármán strain assumption are used to establish the equilibrium equations for the S-FGM nanoplate. The small size-dependents are captured by using nonlocal parameters and strain gradient parameters. This article is structured as follows. Two porosity distribution patterns of the S-FGM nanoplate are introduced in Sections 2; The nonlinear nonlocal strain gradient equilibrium equations based on Reissner-Mindlin plate theory are derived in Section 3; Section 4 present the general governing equation for nonlinear bending of S-FGM nanoplate. The numerical examples and conclusions are presented in the last section.

2. The porous S-FGM nanoplate model

The porosities (micro-voids) may have occurred during the fabrication process wherein the porosities vary across the thickness's direction follow different patterns. As in Fig. 1, this study considers two patterns of porosity distribution. For Pattern A, the porosities are symmetrically varied across the thickness direction and are released at the plate's top and bottom. However, they are enriched in the middle plane. For Pattern B, the porosities concentrate at the upper part of the plate and evenly reduce at the lower part of the plate, and it is means the porosities are asymmetrically varied across the thickness direction.

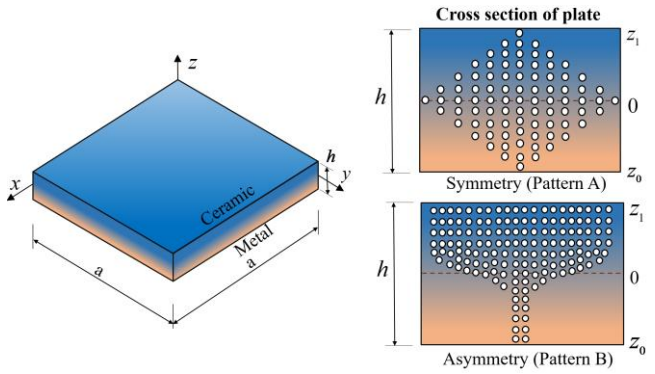

Fig. 1 The configurations of porous S-FGM nanoplate

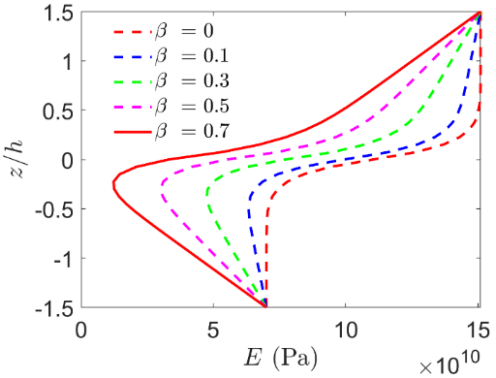

(a) Pattern A

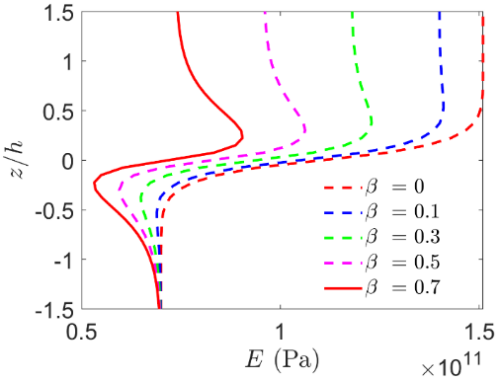

(b) Pattern B

Fig. 2 Young's modulus across the plate's thickness of porous S-FGM (AL/ZrO_2) at n = 10.

Assuming a porous S-FGM nanoplate with thickness h, length a, the efficiency material properties of porous S-FGM nanoplate, including Young's modulus E, and Poisson ratio ν, are defined based on the sigmoid rule of a mixture such as Singh and Harsha (2020):

* Pattern A:

$$\begin{aligned}
\nu_1 &= \nu_c\frac{1}{2}\left(1+\frac{2z}{h}\right)^n+\nu_m\left(1-\frac{1}{2}\left(1+\frac{2z}{h}\right)^n\right)\\
&\quad-(\nu_c+\nu_m)\frac{\beta}{2}\left(1-\frac{2|z|}{h}\right)\ \text{For } 0\le z\le\frac{h}{2}\\
E_2 &= E_c\left(1-\frac{1}{2}\left(1-\frac{2z}{h}\right)^n\right)+E_m\frac{1}{2}\left(1-\frac{2z}{h}\right)^n\\
&-(E_c+E_m)\frac{\beta}{2}\left(1-\frac{2|z|}{h}\right)
\end{aligned}\tag{1}$$

$$\begin{aligned}
\nu_1 &= \nu_c\left(1-\frac{1}{2}\left(1-\frac{2z}{h}\right)^n\right)+\nu_m\frac{1}{2}\left(1-\frac{2z}{h}\right)^n\\
&-(\nu_c+\nu_m)\frac{\beta}{2}\left(1-\frac{2|z|}{h}\right)
\end{aligned}$$

* Pattern B:

$$\begin{aligned}
&\text{For } -\frac{h}{2}\le z\le 0\\
E_1 &= E_c\frac{1}{2}\left(1+\frac{2z}{h}\right)^n+E_m\left(1-\frac{1}{2}\left(1+\frac{2z}{h}\right)^n\right)\\
&\quad-\left(E_c+E_m\right)\frac{\beta}{2}\left(1-\frac{2|z|}{h}\right)\\
\nu_1 &= \nu_c\frac{1}{2}\left(1+\frac{2z}{h}\right)^n+\nu_m\left(1-\frac{1}{2}\left(1+\frac{2z}{h}\right)^n\right)\\
&\quad-\left(\nu_c+\nu_m\right)\frac{\beta}{2}\left(1-\frac{2|z|}{h}\right)\\
&\text{For } 0\le z\le\frac{h}{2}\\
E_2 &= E_c\left(1-\frac{1}{2}\left(1-\frac{2z}{h}\right)^n\right)+E_m\frac{1}{2}\left(1-\frac{2z}{h}\right)^n\\
&-\left(E_c+E_m\right)\frac{\beta}{2}\left(1-\frac{2|z|}{h}\right)\\
\nu_1 &= \nu_c\left(1-\frac{1}{2}\left(1-\frac{2z}{h}\right)^n\right)+\nu_m\frac{1}{2}\left(1-\frac{2z}{h}\right)^n\\
&-(\nu_c+\nu_m)\frac{\beta}{2}\left(1-\frac{2|z|}{h}\right)
\end{aligned}\tag{2}$$

where β is the porosity coefficient that denotes the volume fraction of porosity in the S-FGM nanoplate; n denotes the power index.

For understanding the material properties variation of porous S-FGM, Young's modulus variation across the thickness of AL/ZrO_2 S-FGM are figured out for symmetric and asymmetric porosity distribution as in Fig. 2. It can be seen that the presented porosity S-FGM mathematical equation ensures the continuity of Young's modulus E across the plate's thickness. For different porosity coefficients, the values of E obtained from Pattern A have coincided at the top and bottom of the plate. Unlike the asymmetric porosity distribution, the values of E are separated at the top surface. The higher value of the porosity coefficient causes the lower values of Young's modulus.

3. The S-FGM nanoplate model

3.1 The brief nonlocal strain gradient theory

Based on an experimental study Lam *et al.* (2003), Eringen's nonlocal theory limits predicting the stiffness hardening mechanism. Therefore, Lim *et al.* (2015) presented the nonlocal strain gradient theory that deals with

the nonlocal model and strain gradient model. The stress tensor is defined such as.

$$\boldsymbol{\tau} = \boldsymbol{\tau}^0 - \nabla\boldsymbol{\tau}^1 \tag{3}$$

where, $\boldsymbol{\tau}$ is the total stress tensor; $\boldsymbol{\tau}^0$ and $\boldsymbol{\tau}^1$ are the classical nonlocal stress and the higher-order stress tensors, as given as follows.

$$\begin{aligned}\boldsymbol{\tau}^0 &= \int_\Omega \alpha_0(\boldsymbol{x},\bar{\boldsymbol{x}},e_0a)\,\boldsymbol{\sigma}(\bar{\boldsymbol{x}})d\Omega \\ \boldsymbol{\tau}^1 &= \eta^2\int_\Omega \alpha_1(\boldsymbol{x},\bar{\boldsymbol{x}},e_1a)\,\nabla\boldsymbol{\sigma}(\bar{\boldsymbol{x}})d\Omega\end{aligned} \tag{4}$$

$\alpha_0(\boldsymbol{x},\bar{\boldsymbol{x}},e_0a)$ is the nonlocal attenuation function, and $\alpha_1(\boldsymbol{x},\bar{\boldsymbol{x}},e_1a)$ is denoted the nonlocal effect corresponding to the first order strain gradient field. e_0 and e_1 are related to the nonlocal parameters. $\boldsymbol{\sigma}$ is the local stress tensor associated with the classical continuum theory at a reference material point.

Following Eringen's nonlocal theory, we get

$$\begin{aligned}\boldsymbol{\tau}^0 &= \int_\Omega \alpha_0(\boldsymbol{x},\bar{\boldsymbol{x}},e_0a)\,\boldsymbol{\sigma}(\bar{\boldsymbol{x}})d\Omega \\ \boldsymbol{\tau}^1 &= \eta^2\int_\Omega \alpha_1(\boldsymbol{x},\bar{\boldsymbol{x}},e_1a)\,\nabla\boldsymbol{\sigma}(\bar{\boldsymbol{x}})d\Omega\end{aligned} \tag{5}$$

where the Laplacian operator is $\nabla^2 = \frac{\partial^2}{\partial x^2} + \frac{\partial^2}{\partial y^2}$.

By applying the differential operators $\Im_0 = 1 - (e_0a)^2\nabla^2$ on both sides of Eq. (3), together with the using Eq. (5), we get

$$(1-(e_0a)^2\nabla^2)\boldsymbol{\tau} = \boldsymbol{\sigma} - (1-(e_0a)^2\nabla^2)\nabla\boldsymbol{\tau}^{(1)} \tag{6}$$

By applying the operator $\Im_1 = 1 - (e_1a)^2\nabla^2$ to Eq. (6), together with Eq. (5), the general nonlocal constitutive equations are obtained as the following form.

$$\begin{aligned}&(1-(e_1a)^2\nabla^2)(1-(e_0a)^2\nabla^2)\tau = \\ &(1-(e_1a)^2\nabla^2)\sigma - \eta^2(1-(e_0a)^2\nabla^2)\nabla^2\sigma\end{aligned} \tag{7}$$

By assuming $e_0 = e_1 = e$, Eq. (7) is rewritten as

$$(1-\mu\nabla^2)\boldsymbol{\tau} = (1-\ell\nabla^2)\boldsymbol{\sigma} \tag{8}$$

In which, $\mu = (ea)^2$ and $\ell = \eta^2$ are defined as the nonlocal parameter and gradient parameter, respectively.

The nonlocal equation of motion for the linear elasticity constitution of the nanoscale solid is given as Eringen and Edelen (1972), Eringen (1972).

$$\rho\ddot{\boldsymbol{u}} - \nabla\cdot\boldsymbol{\tau} - \boldsymbol{b} = \boldsymbol{0} \quad \text{in a domain } \Omega \tag{9}$$

where ρ and $\ddot{\boldsymbol{u}}$ denote mass density and accelerator component at a reference material point; $\boldsymbol{\tau}$, and **b** are the stress tensor and body force, respectively.

From Eqs. (8) and (9), the nonlocal strain gradient differential constitutive equations can be defined in the following form.

$$\begin{aligned}&(1-\mu\nabla^2)\rho\ddot{\boldsymbol{u}} - (1-\ell\nabla^2)\nabla\cdot\boldsymbol{\sigma} - (1-\mu\nabla^2)\boldsymbol{b} \\ &= 0 \quad \text{on } \Omega\end{aligned} \tag{10}$$

By applying the variational principle, the weak form formulation for nanoplate can be obtained as follows.

$$\begin{aligned}&\int_\Omega \delta\boldsymbol{u}\cdot(1-\mu\nabla^2)\rho\ddot{\boldsymbol{u}}d\Omega - \int_\Omega \delta\boldsymbol{u}\cdot(1-\ell\nabla^2)\nabla\cdot\boldsymbol{\sigma}d\Omega - \\ &\int_\Omega \delta\boldsymbol{u}\cdot(1-\mu\nabla^2)\boldsymbol{b}d\Omega = 0\end{aligned} \tag{11}$$

By using the divergence theorem and ignoring the traction on the Neumann boundary, Eq. (11) is rewritten as follows.

$$\begin{aligned}&\int_\Omega \delta\boldsymbol{u}\cdot(1-\mu\nabla^2)\rho\ddot{\boldsymbol{u}}d\Omega + \int_\Omega \delta\boldsymbol{\varepsilon}:(1-\ell\nabla^2)\boldsymbol{\sigma}d\Omega - \\ &\int_\Omega \delta\boldsymbol{u}\cdot(1-\mu\nabla^2)\boldsymbol{b}d\Omega = 0\end{aligned} \tag{12}$$

3.2 The Reissner -Mindlin plate theory

The displacement field of an arbitrary point in the plate domain $V = \Omega x\left(\frac{-h}{2},\frac{h}{2}\right)$ of Reissner-Mindlin plate theory is expressed as follows (Reddy 2004).

$$\hat{u} = u_1 + zu_2 \tag{13}$$

In which $\hat{u} = \{u\ v\ w\}^T$ is the displacement of a point in plate domain; $u_1 = \{u_0\ v_0\ w_0\}^T$ is represents the displacements of the middle plane; $u_2 = \{\beta_x\ \beta_y\ 0\}^T$ is the vector of rotations.

The strain components based on the Reissner-Mindlin plate theory with Von-Kármán strain assumption are established, such as

$$\begin{aligned}&\varepsilon = \{\varepsilon_x\ \varepsilon_y\ \gamma_{xy}\}^T = \varepsilon_0 + z\kappa_1; \\ &\varepsilon_o = \varepsilon_0^L + \varepsilon_0^{NL} = \begin{Bmatrix} u_{0,x} \\ v_{0,y} \\ u_{0,y}+v_{0,x}\end{Bmatrix} + \frac{1}{2}\begin{Bmatrix} w_{0,x}^2 \\ w_{0,y}^2 \\ 2w_{0,x}w_{0,y}\end{Bmatrix}; \\ &\kappa_1 = \begin{Bmatrix} \beta_{x,x} \\ \beta_{y,y} \\ \beta_{x,y}+\beta_{y,x}\end{Bmatrix};\ \gamma = \{\gamma_{xz}\ \gamma_{yz}\}^T = \begin{Bmatrix}\beta_x + w_{0,x} \\ \beta_y + w_{0,y}\end{Bmatrix}\end{aligned} \tag{14}$$

Consequently, the local constitutive stress-strain relations are presented as

$$\begin{aligned}&\hat{\sigma} = \begin{Bmatrix} N^u \\ M^u \\ E^u\end{Bmatrix} = \begin{bmatrix} K & L & 0 \\ L & U & 0 \\ 0 & 0 & W\end{bmatrix}\begin{Bmatrix}\varepsilon_0 \\ \kappa_1 \\ \gamma\end{Bmatrix} = \widehat{\mathfrak{K}}_u\hat{\varepsilon}; \\ &(K,L,U) = \sum_{i=1}^{N}\int_{\frac{-h_i}{2}}^{\frac{h_i}{2}}(1,z,z^2)\,C dz; \\ &W = \sum_{i=1}^{N}\int_{\frac{-h_i}{2}}^{\frac{h_i}{2}}\frac{E_i(z)}{2(1+\nu_i(z))}\begin{bmatrix}1 & 0 \\ 0 & 1\end{bmatrix}dz; \\ &C = \frac{E_i(z)}{1+\nu_i(z)}\begin{bmatrix}\frac{1}{1-\nu_i(z)} & \frac{\nu_i(z)}{1-\nu_i(z)} & 0 \\ \frac{\nu_i(z)}{1-\nu_i(z)} & \frac{1}{1-\nu_i(z)} & 0 \\ 0 & 0 & \frac{1}{2}\end{bmatrix}\end{aligned} \tag{13}$$

Replacing Eq. (15) into Eq. (12) and eliminating the first term, the weak form formulation for nonlinear static bending of S-FGM nanoplate is established, such as

$$\int_{\Omega} \delta\hat{\varepsilon}^T \widehat{\mathfrak{K}}_u (1-\ell\nabla^2)\hat{\varepsilon} d\Omega = \int_{\Omega} \delta\hat{u}(1-\mu\nabla^2)\boldsymbol{b} d\Omega \quad (16)$$

4. Nonlinear governing equations based NURBS formulation

4.1 Governing equations

The classical FEM approximates the known geometry and the unknown fields using Lagrange basic functions. So, this method sustains a geometrical error because of the difference between CAD and the analysis model. However, isogeometric analysis utilizes B-spline or NURBS as a basic function to accurately capture the geometry. Therefore, the accuracy of geometry is ensured at all phases of the analysis process. NURBS also is used to approximate the displacement fields based on the shear deformation theory, such as (Thanh *et al*. 2019a, b, c)

$$u^h(\hat{\xi}) = \sum_{I}^{A} \mathbb{R}_I(\hat{\xi}) d_I \quad (17)$$

where $d_I = \{u_{0I} \quad v_{0I} \quad w_{0I} \quad \beta_{xI} \quad \beta_{yI}\}^T$, $\mathbb{R}_I$, respectively, are the vector of a degree of freedoms associated with the control point $\mathbf{P}_I$ and the NURBS basic functions. *A* is the number of control points.

Substituting Eq. (17) into Eq. (14), the general in-plane strain can be rewritten in a matrix form as:

$$\begin{aligned} \hat{\varepsilon} &= \hat{\varepsilon}_L + \hat{\varepsilon}_{NL} = \{\varepsilon_0^L \quad \kappa_1 \quad \gamma\}^T + \{\varepsilon_0^{NL} \quad 0 \quad 0\}^T \\ &= \sum_{I=1}^{m\times n} \left(\hat{B}_I^L + \frac{1}{2}B_I^{NL}\right) d_I \end{aligned} \quad (18)$$

in which,

$$\begin{aligned} \hat{B}_I^L &= [(B_I^m)^T \quad (B_I^b)^T \quad (B_I^s)^T]^T \\ B_I^m &= \begin{bmatrix} \mathbb{R}_{I,x} & 0 & 0 & 0 \\ 0 & \mathbb{R}_{I,y} & 0 & 0 & 0 \\ \mathbb{R}_{I,y} & \mathbb{R}_{I,x} & 0 & 0 & 0 \end{bmatrix}; \\ B_I^b &= \begin{bmatrix} 0 & 0 & 0 & \mathbb{R}_{I,x} & 0 \\ 0 & 0 & 0 & 0 & \mathbb{R}_{I,y} \\ 0 & 0 & 0 & \mathbb{R}_{I,y} & \mathbb{R}_{I,x} \end{bmatrix}; \\ B_I^s &= \begin{bmatrix} 0 & 0 & \mathbb{R}_{I,x} & \mathbb{R}_I & 0 \\ 0 & 0 & \mathbb{R}_{I,y} & 0 & \mathbb{R}_I \end{bmatrix} \end{aligned} \quad (19)$$

The strain matrix due to the nonlinear strain is formulated as

$$\begin{aligned} B_I^{NL}(d) &= \begin{bmatrix} \Im_\theta \\ 0 \end{bmatrix} B_I^g \\ where\ B_I^g &= \begin{bmatrix} 0 & 0 & \mathbb{R}_{I,x} & 0 & 0 \\ 0 & 0 & \mathbb{R}_{I,y} & 0 & 0 \end{bmatrix}; \\ \Im_\theta &= \begin{bmatrix} w_{0,x} & 0 \\ 0 & w_{0,y} \\ w_{0,y} & w_{0,x} \end{bmatrix} \end{aligned} \quad (20)$$

Replacing Eq. (18) into Eqs. (16), the global equilibrium equations for nonlinear static bending responses of S-FGM nanoplate can be established, such as

$$\begin{aligned} &(K_L + K_{NL})d = f \\ &K = \int_{\Omega} \hat{B}^T \widehat{\mathfrak{K}}_u \left(\hat{B} - \ell\nabla^2\hat{B}\right) d\Omega; \\ &f = \int_{\Omega} f_0(1-\mu\nabla^2)\{0 \quad 0 \quad w_I \quad 0 \quad 0\}^T d\Omega\,. \end{aligned} \quad (21)$$

In which, K_L and K_{NL} are the general linear and nonlinear stiffness matrix, respectively, as defined as follows

$$\begin{aligned} K^L &= \int_{\Omega} \hat{B}^L \widehat{\mathfrak{K}}_u \left(\hat{B}^L - \ell\nabla^2\hat{B}^L\right) d\Omega; \\ K^{NL} &= \frac{1}{2}\int_{\Omega} \hat{B}^L \widehat{\mathfrak{K}}_u \left(\hat{B}^{NL} - \ell\nabla^2\hat{B}^{NL}\right) d\Omega \\ &+ \int_{\Omega} \hat{B}^{NL} \widehat{\mathfrak{K}}_u \left(\hat{B}^L - \ell\nabla^2\hat{B}^L\right) d\Omega \\ &+ \frac{1}{2}\int_{\Omega} \hat{B}^{NL} \widehat{\mathfrak{K}}_u \left(\hat{B}^{NL} - \ell\nabla^2\hat{B}^{NL}\right) d\Omega \end{aligned} \quad (22)$$

The general forces vector f is formulated as

$$f = \int_{\Omega} f_0(1-\mu\nabla^2)\{0 \quad 0 \quad w_I \quad 0 \quad 0\}^T d\Omega \quad (23)$$

4.2 Nonlinear procedure

The Newton-Raphson iteration is adopted to obtain the iterative responses of Eq. (21). At a load level m^{th}, the residual force $\mathbf{R}(\mathbf{d}^i)$ at i^{th} iteration is defined such as

$$R(d^i) = \left(K_L + K_{NL}(d^i)\right) - F^m \quad (24)$$

At $(i+1)^{\text{th}}$ iteration, the displacement is defined as follows

$$d^{i+1} = d^i + \Delta d^{i+1} \quad (25)$$

The increment displacement Δd^{i+1} for i^{th} iteration is defined such as:

$$\Delta d^{i+1} = -K_T^{-1} R(d^i) \quad (26)$$

The tangent stiffness K_T is calculated as

$$\begin{aligned} K_T(d^i) &= \frac{\partial R(d^i)}{\partial d^i} = \widetilde{K}_{NL} + K_g \\ \widetilde{K}_{NL} &= \int_{\Omega} \hat{B}^L \widehat{\mathfrak{K}}_u \left(\hat{B}^L - \ell\nabla^2\hat{B}^L\right) d\Omega \\ &+ \int_{\Omega} \hat{B}^L \widehat{\mathfrak{K}}_u \left(\hat{B}^{NL} - \ell\nabla^2\hat{B}^{NL}\right) d\Omega \\ &+ \int_{\Omega} \hat{B}^{NL} \widehat{\mathfrak{K}}_u \left(\hat{B}^L - \ell\nabla^2\hat{B}^L\right) d\Omega \\ &+ \int_{\Omega} \hat{B}^{NL} \widehat{\mathfrak{K}}_u \left(\hat{B}^{NL} - \ell\nabla^2\hat{B}^{NL}\right) d\Omega \end{aligned} \quad (27)$$

K_g is the geometric stiffness matrix corresponding to the in-plane stresses N_x, N_y, N_{xy}, which is defined as follows

$$K_g = \int_{\Omega} (\mathbb{N}^g)^T \begin{bmatrix} N_x & N_{xy} \\ N_{xy} & N_y \end{bmatrix} (\mathbb{N}^g) d\Omega \quad (28)$$

The iteration is repeated until the difference of displacement between the two steps is small enough.

Table 1 Comparison deflection of isotropic square nanoplate

μ	a/h = 10			a/h = 100		
	Lee *et al*. (2012	Jung and Han (2013)	Present	Lee *et al*. (2012)	Jung and Han (2013)	Present
0	4.6658	4.6658	4.6659	4.4384	4.4384	4.4384
0.5	5.0836	5.0836	5.0838	4.8408	4.8408	4.8408
1	5.5014	5.5012	5.5016	5.2432	5.2432	5.2432
1.5	5.9192	5.9189	5.9195	5.6456	5.6456	5.6456
2	6.3370	6.3365	6.3373	6.0480	6.0480	6.0479
2.5	6.7548	6.7542	6.7552	6.4504	6.4504	6.4503
3	7.1726	7.1718	7.1730	6.8528	6.8528	6.8527
3.5	-	7.5895	7.5909	-	7.2552	7.2551
4	-	8.0071	8.0088	-	7.6576	7.6575

Table 2 The nonlocal effect on a deflection $\bar{w}$ of SSSS AL/Al_2O_3 nanoplate

Method	n	a/h = 10			a/h = 50		
		μ			μ		
		0	1	4	0	1	4
Nguyen *et al*. (2015)	0	0.0787	0.0928	0.1351	0.0750	0.0886	0.1294
Present		0.0787	0.0928	0.1351	0.0750	0.0886	0.1294
Nguyen *et al*. (2015)	1	0.1977	0.2331	0.3393	0.1888	0.2230	0.3256
Present		0.1971	0.2325	0.3385	0.1887	0.2229	0.3256
Nguyen *et al*. (2015)	2	0.2344	0.2763	0.4021	0.2222	0.2625	0.3834
Present		0.2329	0.2747	0.3999	0.2222	0.2625	0.3833
Nguyen *et al*. (2015)	5	0.2730	0.3217	0.4678	0.2564	0.3028	0.4422
Present		0.2706	0.3189	0.4641	0.2563	0.3027	0.4421
Nguyen *et al*. (2015)	10	0.3052	0.3597	0.5231	0.2869	0.3390	0.4950
Present		0.3034	0.3577	0.5204	0.2869	0.3389	0.4949

5. Numerical examples

Numerical results are presented to explore the influence of porosity coefficient, the pattern of porosity distribution, power index *n*, nonlocal parameter, strain gradient parameter on linear and nonlinear behaviors of porous S-FGM nanoplate. From Eq. (22), the higher-order derivative of the NURBS basic function is required. Therefore, the cubic NURBS function with the meshes element 11×11 is utilized in this study, and this type of meshes element proved its convergence through the published work (Thanh *et al*. 2019a, b). In this study, the sigmoid AL/ZrO_2 is used in numerical results, wherein the material of aluminum (AL) and zirconia (ZrO_2) are $E_m = 70GPa, \nu_m = 0.3$ for Al and $E_c = 151GPa,\ \nu_c = 0.3$ for ZrO_2. Also, for convenience, the nonlocal and strain gradient parameters are normalized as $\frac{\sqrt{\mu}}{a}$ and $\frac{\sqrt{\ell}}{a}$, respectively.

5.1 Verification study

Several numerical examples are investigated to verify the presented numerical model for linear and nonlinear analysis of S-FGM nanoplate. The comparison results are exhibited in tables and figures.

Firstly, the validity and reliability of the presented solution are started with evaluating the influence of nonlocal parameters on the linear static bending of an isotropic simply-supported nanoplate. Table 1 tabulates the non-dimensional deflection $\bar{w} = \frac{100Eh^3w_0}{(q_0a^4)}$ of isotropic nanoplate, in which the material properties of nanoplate is chosen such as $E_m = 30 \times 10^6 Pa,\ \nu = 0.3$. The obtained results are compared with those derived by the analytical solution of Jung and Han (2013) and the third-order shear deformation nonlocal analytical solution by Lee *et al*. (2012). It can be observed that the presented results give similar values even with aspect ratio a/h = 10 and a/h = 100.

Secondly, Table 2 compares the central deflection $\bar{w} = \frac{100E_mh^3w_0}{\left(12(1-\nu_m^2)\right)}$ for FGM nanoplate with the material properties modulus $E_m = 70\ GPa,\ E_c = 380\ GPa$ and $\nu_c = \nu_m = 0.3$. The nanoplate is subjected to uniform load q_0 with simply-supported boundary. The refined plate quasi-3D theory nonlocal solution established by Nguyen *et al*. (2015) is used for comparison purposes. For various values of nonlocal parameters $\mu = 0, 1, 4$, there is no difference in deflection for power index n = 0. However, the results depict a slight difference in deflection for n = 1, 2, 5, 10, and

Table 3 The strain gradient effect on a deflection $\bar{w}$ of SSSS isotropic nanoplate

Method	n	$\sqrt{\ell}$			
		0	0.2	0.5	1
Thai *et al*. (2020)	5	4.9027	4.8689	4.6953	4.1448
Present		4.9043	4.8755	4.7327	4.1930
Thai *et al*. (2020)	10	4.2651	4.2421	4.0867	3.5993
Present		4.2728	4.2440	4.1003	3.6183
Thai *et al*. (2020)	50	4.0708	4.0414	3.8916	3.4211
Present		4.0708	4.0420	3.8982	3.4588
Thai *et al*. (2020)	100	4.0645	4.0352	3.8859	3.4086
Analytical (Babu and Patel 2019)		4.0624	4.0330	3.8844	3.4231
FEM-C (Babu and Patel 2019)		4.0624	4.0332	3.8856	3.4271
Present		4.0645	4.0359	3.8937	3.4608

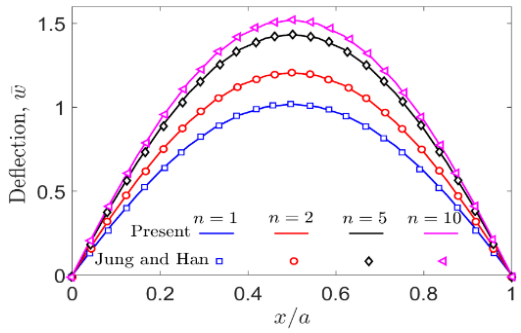

Fig. 3 The non-dimensional deflection of the S-FGM square plate along the *x*-direction at *y* = *b*/2

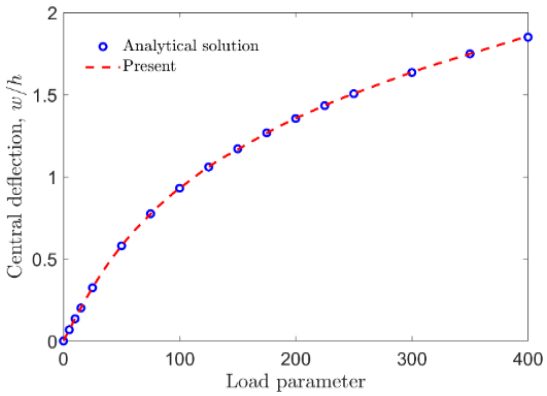

Fig. 4 Nonlinear deflection of clamped isotropic square plate

it is observed that the maximum difference is about 0.88%.

Thirdly, in order to compare the deflection of nanoplate under strain gradient influence, Table 3 shows the deflection $\bar{w} = \frac{100wD}{(q_0 a^4)}$, D=$\frac{Eh^3}{(12(1-\nu^2))}$ for a simply-supported nanoplate with the material properties $E = 30 \times 10^6 Pa, \nu = 0.3$. For various values of strain gradient parameter $(\sqrt{\ell} = 0, 0.2, 0.5, 1)$, it can be seen that the presented results show excellent agreement in comparison with those solved by Thai *et al*. (2020), Babu and Patel (2019).

Fourthly, due to the limited solution for static bending of S-FGM nanoplate, the central deflections of S-FGM

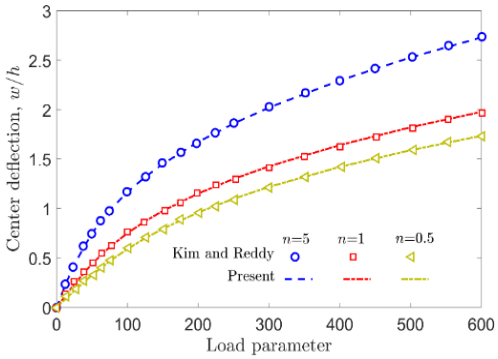

Fig. 5 The effect of power index *n* on nonlinear responses of FG plate

based on classical continuum elastic theory are plotted in Fig. 3. The obtained deflections along *x*-direction at *y* = *a*/2 are compared with those results given by Jung and Han (2013). It can be seen that the higher power index *n* leads to the higher deflection, and the presented results show an excellent agreement with reference solution for various values of power index *n* = 1, 2, 5, 10.

Fifthly, this study aims to verify the accuracy of the presented solution in solving the nonlinear bending responses plate. A clamped isotropic with aspect ratio *a*/*h*=100, $E = 30 \times 10^6 Psi, \nu = 0.316$ is investigated. Under the uniform loading, the non-dimensional central deflection $\frac{w}{h}$ versus load parameter $\bar{P} = \frac{q_0 a^4}{(E_m h^4)}$ curves are plotted in Fig. 4. An excellent agreement of the presented solution is found by comparing the solution established by Levy and Chiarito (1942).

Next, another functionally graded plate is investigated to examine the accuracy of the presented solution further. The plate is subjected simply supported boundary condition with the material properties E_1 = 14.4 GPa, E_2= 1.44 GPa, and ν = 0.38. The obtained load parameter $\bar{P} = \frac{q_0 L^4}{(E_2 h^4)}$ versus deflection curves for various values of power index n = 0.5, 1, 5 is compared with those derived from Kim and Reddy (2015). It is observed that the center deflection for every load parameter gives the same value as the reference solution.

Table 4 Central deflection of porous S-FGM nanoplate with various small size parameters

$\frac{\sqrt{\mu}}{a}$	$\frac{\sqrt{\ell}}{a}$	Perfect	Pattern A			Pattern B		
			$\beta = 0.2$	$\beta = 0.5$	$\beta = 0.7$	$\beta = 0.2$	$\beta = 0.5$	$\beta = 0.7$
0	0	0.4296	0.4650	0.5313	0.5894	0.4700	0.5492	0.6253
	0.1	0.3590	0.3887	0.4440	0.4926	0.3928	0.4590	0.5226
	0.2	0.2415	0.2615	0.2987	0.3314	0.2643	0.3089	0.3518
	0.3	0.1570	0.1700	0.1942	0.2155	0.1718	0.2009	0.2288
	0.4	0.1056	0.1143	0.1306	0.1449	0.1156	0.1352	0.1540
0.1	0	0.5144	0.5568	0.6361	0.7057	0.5628	0.6576	0.7487
	0.1	0.4299	0.4654	0.5316	0.5898	0.4703	0.5496	0.6258
	0.2	0.2892	0.3131	0.3577	0.3969	0.3165	0.3699	0.4212
	0.3	0.1880	0.2035	0.2325	0.2580	0.2057	0.2405	0.2739
	0.4	0.1264	0.1369	0.1564	0.1736	0.1384	0.1618	0.1844
0.2	0	0.7688	0.8322	0.9507	1.0547	0.8411	0.9829	1.1190
	0.1	0.6425	0.6955	0.7946	0.8815	0.7029	0.8215	0.9353
	0.2	0.4323	0.4680	0.5346	0.5931	0.4730	0.5528	0.6295
	0.3	0.2809	0.3042	0.3475	0.3856	0.3074	0.3595	0.4094
	0.4	0.1889	0.2046	0.2338	0.2594	0.2068	0.2419	0.2756
0.3	0	1.1928	1.2912	1.4750	1.6364	1.3049	1.5249	1.7362
	0.1	0.9969	1.0791	1.2328	1.3676	1.0906	1.2745	1.4511
	0.2	0.6707	0.7261	0.8295	0.9202	0.7338	0.8577	0.9767
	0.3	0.4359	0.4719	0.5392	0.5982	0.4770	0.5577	0.6352
	0.4	0.2931	0.3174	0.3627	0.4024	0.3209	0.3753	0.4276
0.4	0	1.7863	1.9338	2.2091	2.4507	1.9543	2.2838	2.6002
	0.1	1.4929	1.6162	1.8463	2.0482	1.6334	1.9088	2.1732
	0.2	1.0044	1.0874	1.2423	1.3782	1.0990	1.2845	1.4627
	0.3	0.6528	0.7068	0.8075	0.8959	0.7144	0.8353	0.9514
	0.4	0.4390	0.4754	0.5432	0.6027	0.4806	0.5621	0.6404

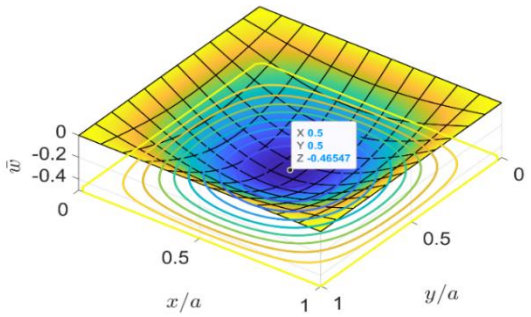

Fig. 6 Deflection of porous S-FGM nanoplate (Pattern A) with $\frac{\sqrt{\mu}}{a} = \frac{\sqrt{\ell}}{a} = 0.1$

5.2 Parameter study to porous S-FGM nanoplate

In this example, the simply supported AL/ZrO2 porous S-FGM nanoplate is considered. The parameter studies are investigated to examine the influence of porosity coefficient, the pattern of porosity distribution, aspect ratio, power index, nonlocal and strain gradient parameters on porous S-FGM's linear and static bending responses.

The values of non-dimensional deflection $\bar{w} = \frac{10^2 E_c h^3}{(q_0 a^4)}$ corresponding to various values of the nonlocal parameter and strain gradient parameter for pattern B and pattern B dispersion porosity are tabulated in Table 4 to indicate the effect of small size parameter on the linear deflection of porous S-FGM nanoplate with power index n =10 and aspect ratio a/h = 20. The value $\beta = 0$ indicates the perfect type of porosity, in which the influence of porosity is ignored. It can be known that the non-dimensional deflection increases with an increase in porosity coefficient. The type of perfect porosity gives the lowest value of deflection of S-FGM nanoplate. It can be known as the existence of porosity leading to the reduction in plate's stiffness. When the porosity coefficient β rises from 0.2 to 0.7, the non-dimensional deflection increases by 8.25%, 23.66%, and 37,195% with $\frac{\sqrt{\mu}}{a} = \frac{\sqrt{\ell}}{a} = 0.1$ for the case of Pattern A. Also, asymmetric porosity distribution generates higher deflection values than symmetric porosity distribution at a specific porosity coefficient. Furthermore, the augmentation in the values $\bar{w}$ is due to the nonlocal effect, but the strain gradient effect reduces deflection. Fig. 6 shows the variation of S-FGM nanoplate corresponding to Pattern A with $\frac{\sqrt{\mu}}{a} = \frac{\sqrt{\ell}}{a} = 0.1$, $n = 10$, $\beta = 0.2$.

Table 5 Central deflection of porous S-FGM nanoplate with various aspect ratio *a*/*h*

a/*h*	*n*	Perfect	Pattern A			Pattern B		
			$\beta = 0.2$	$\beta = 0.5$	$\beta = 0.7$	$\beta = 0.2$	$\beta = 0.5$	$\beta = 0.7$
10	0	0.4038	0.4294	0.4728	0.5060	0.4561	0.5589	0.6523
	1	0.4217	0.4521	0.5060	0.5500	0.4779	0.5897	0.6929
	2	0.4326	0.4659	0.5266	0.5780	0.4881	0.5968	0.6951
	5	0.4423	0.4783	0.5453	0.6038	0.4901	0.5812	0.6627
	10	0.4453	0.4821	0.5511	0.6118	0.4869	0.5687	0.6473
20	0	0.3884	0.4127	0.4534	0.4840	0.4394	0.5396	0.6306
	1	0.4064	0.4354	0.4865	0.5280	0.4613	0.5704	0.6713
	2	0.4172	0.4492	0.5072	0.5560	0.4715	0.5776	0.6735
	5	0.4269	0.4616	0.5259	0.5818	0.4735	0.5621	0.6412
	10	0.4299	0.4654	0.5316	0.5898	0.4703	0.5496	0.6258
50	0	0.3842	0.4081	0.4480	0.4779	0.4348	0.5343	0.6246
	1	0.4021	0.4308	0.4812	0.5219	0.4567	0.5651	0.6653
	2	0.4130	0.4446	0.5018	0.5499	0.4669	0.5723	0.6676
	5	0.4227	0.4570	0.5206	0.5757	0.4690	0.5568	0.6353
	10	0.4257	0.4608	0.5263	0.5837	0.4658	0.5444	0.6199
100	0	0.3836	0.4075	0.4473	0.4771	0.4342	0.5336	0.6238
	1	0.4015	0.4302	0.4805	0.5211	0.4561	0.5644	0.6645
	2	0.4124	0.4440	0.5011	0.5491	0.4663	0.5716	0.6668
	5	0.4221	0.4564	0.5198	0.5749	0.4684	0.5561	0.6346
	10	0.4251	0.4602	0.5256	0.5829	0.4652	0.5437	0.6191

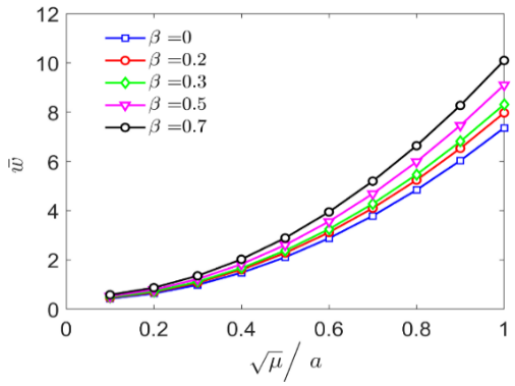

Fig. 7 Effect of nonlocal parameter on the deflection of porous S-FGM nanoplate (Pattern A)

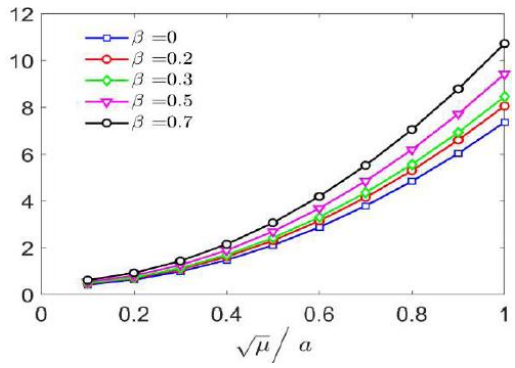

Fig. 8 Effect of nonlocal parameter on the deflection of porous S-FGM nanoplate (Pattern B)

Table 5 tabulates the central deflection of S-FGM nanoplate at size parameters $\frac{\sqrt{\mu}}{a} = \frac{\sqrt{\ell}}{a} = 0.1$ for different values of power index *n* and aspect ratio *a*/*h*. For a given value of aspect ratio *a*/*h* = 10 and $\beta = 0$, the deflection increases 10.27% when *n* increases from 0 to 10. For S-FGM nanoplate with *a*/*h* = 10, by taking $\beta = 0.2$ and $\beta = 0.7$, when increasing *n* from 0 to 10, the deflection of Pattern A increases by 12.27% and 20.9%, respectively. However, there are different responses of deflection for Pattern B as increasing power index *n*. For $\beta = 0.7$, the deflection increases from 0.6523 to 0.6951 when *n* increases from 0 to 2, after that decreasing from 0.6951 to 0.6473 when *n* increases from 2 to 10. At the lower value of porosity coefficient, this unusual behavior happens at the higher value of *n*. It is also revealed from Table 5 that the higher aspect ratio produces the lower deflection, and this change seems to be stable at a higher value of *a*/*h*.

Fig. 7 and 8 illustrate the influence of nonlocal parameters on central deflection of square S-FGM nanoplate corresponding to Pattern A and Pattern B, respectively. It is observed that, at a specific value of the nonlocal parameter $\frac{\sqrt{\mu}}{a}$, the porosity coefficient cause to increase in deflection. For different values of porosity coefficient $\beta = 0, 0.2, 0.3, 0.5, 0.$, the higher value $\frac{\sqrt{\mu}}{a}$ generates the higher values of deflection. The nonlocal coefficient $\frac{\sqrt{\mu}}{a} = 1$ together with $\beta = 0.7$ causes the highest non-deflection.

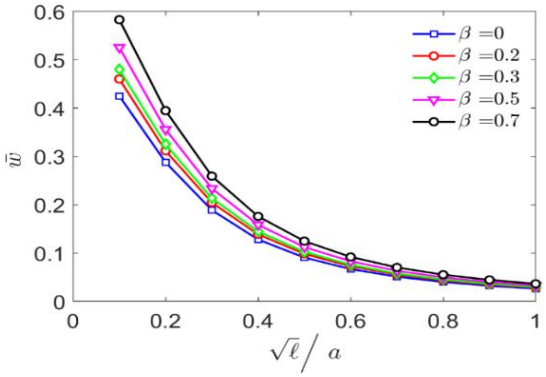

Fig. 9 Effect of gradient parameter on the deflection of porous S-FGM nanoplate (Pattern A)

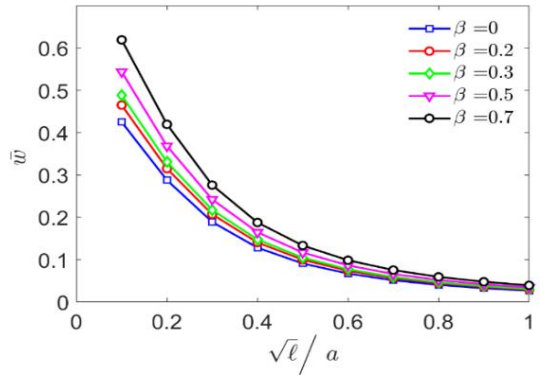

Fig. 10 Effect of gradient parameter on the deflection of porous S-FGM nanoplate (Pattern B)

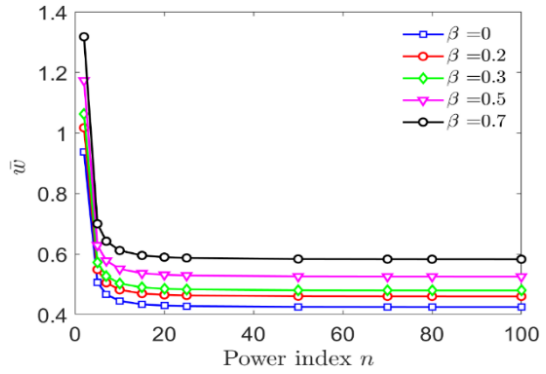

Fig. 11 Effect of power index n on the deflection of porous S-FGM nanoplate (Pattern A)

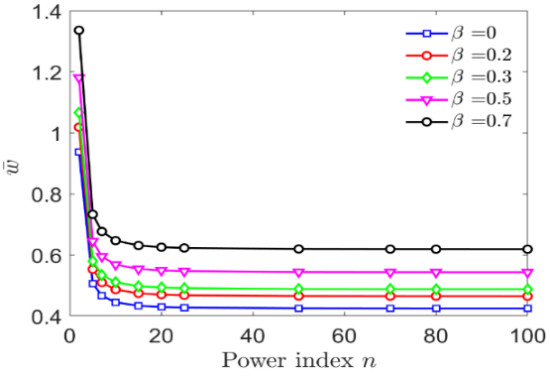

Fig. 12 Effect of power index n on the deflection of porous S-FGM nanoplate (Pattern B)

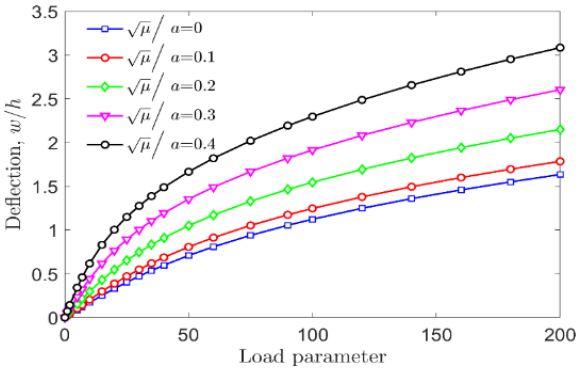

Fig. 13 Effect of nonlocal parameter on nonlinear bending of porous S-FGM nanoplate (Pattern A)

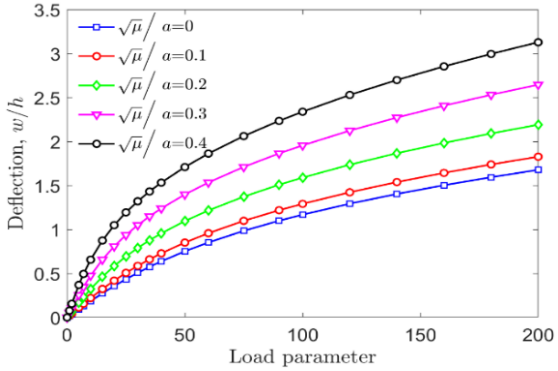

Fig. 14 Effect of nonlocal parameter on nonlinear bending of porous S-FGM nanoplate (Pattern B)

Fig. 9 and 10 depict the variation of non-dimensional deflection of porous S-FGM nanoplate in changing of different values of gradient parameter $\frac{\sqrt{\ell}}{a}$ and porosity coefficient β for Pattern A and Pattern B, respectively. It can be figured out that the variations of deflection are nonlinear instantaneous changes of gradient parameters. For a given value of β, the highest value of deflection is found at $\frac{\sqrt{\ell}}{a} = 0$, while $\frac{\sqrt{\ell}}{a} = 1$ causes the smallest deflection values, the higher value of gradient parameter the lower values of deflection. A higher β value leads to a higher deflection for a specific value $\frac{\sqrt{\ell}}{a}$. In other words, the plate's stiffness is enhanced and weakened due to the strain gradient effect and the porosity coefficient effect, respectively. In Fig. 11 and 12, the effects of aspect ratio a/h on the central deflection at $\frac{\sqrt{\mu}}{a} = \frac{\sqrt{\ell}}{a} = 0.1$ are illustrated for Pattern A and Pattern B, respectively. It can be seen that there is a reduction in deflection from aspect ratio a/h from 2 to 20 after this trend come to stable, and deflection is almost constant. With the increase in the porosity coefficient, the lower responses of deflection are obtained.

Next, we study the nonlinear responses of porous S-FGM under the effect of nonlocal, strain gradient, porosity coefficients, and porosity distribution. The simply-supported plate subjected sinusoidal distributed load $q = q_0 \sin\left(\frac{\pi x}{a}\right) \sin\left(\frac{\pi y}{a}\right)$ is considered. Figs. 13 and 14 plot the

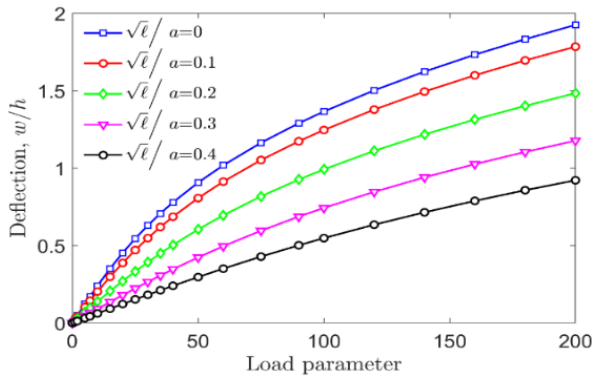

Fig. 15 Effect of strain gradient parameter on nonlinear bending of porous S-FGM nanoplate (Pattern A)

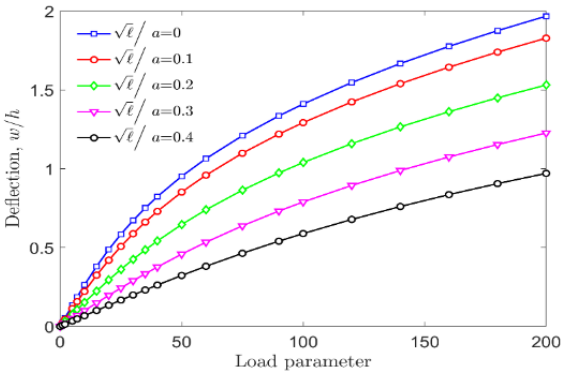

Fig. 16 Effect of strain gradient parameter on nonlinear bending of porous S-FGM (Pattern B)

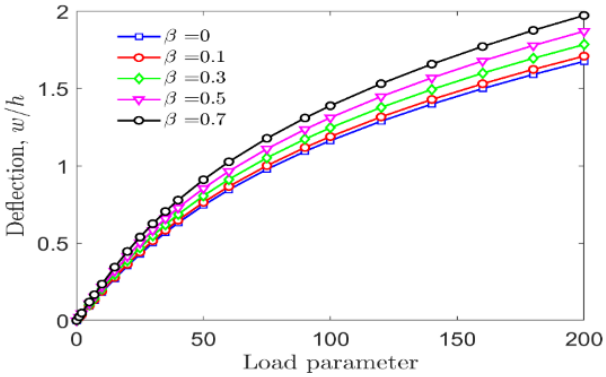

Fig. 17 Effect of porous parameter on nonlinear bending of porous S-FGM nanoplate (Pattern A)

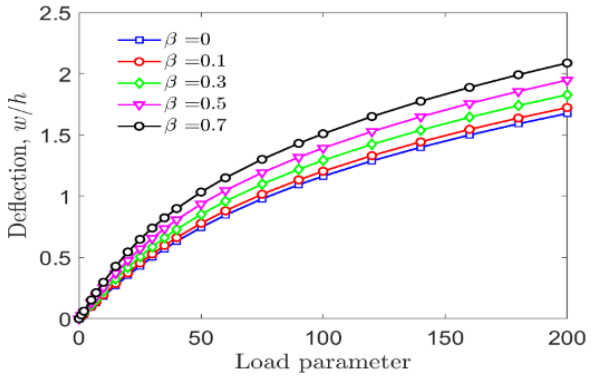

Fig. 18 Effect of porous parameter on nonlinear bending of porous S-FGM nanoplate (Pattern B)

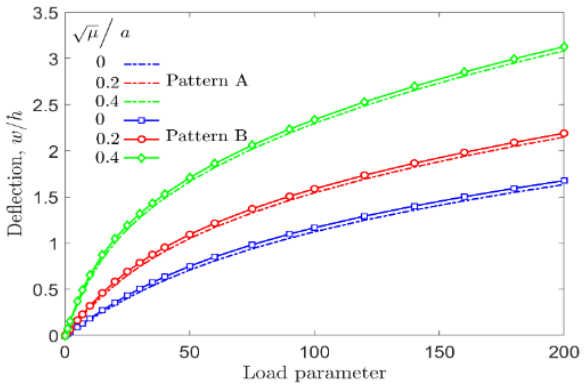

Fig. 19 The influence of porosity distribution pattern on the nonlinear bending for porous corresponding to different nonlocal parameter

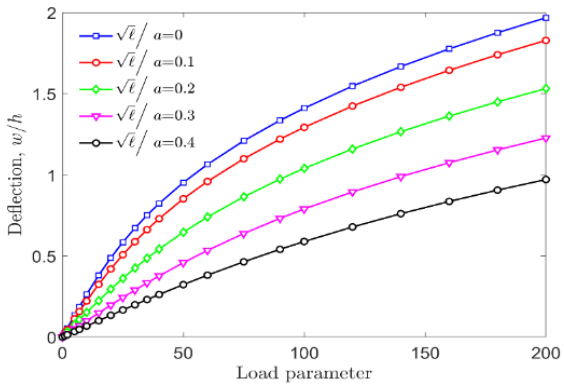

Fig. 20 The influence of porosity distribution pattern on the nonlinear bending for porous corresponding to different strain gradient parameters

deflection $\bar{w} = \frac{w}{h}$ versus load parameter $\bar{w} = \frac{q_0 a^4}{(E_m h^4)}$ for different values of nonlocal parameters corresponding to Pattern A and Pattern B. At a specific value of load parameter, the nonlinear deflection increases with an increase in nonlocal parameter $\frac{\sqrt{\mu}}{a}$. The variance of deflection is nonlinear due to the increase of load parameters. Unlike the nonlocal effect, Figs. 15 and 16 present opposite deflection responses under the strain gradient effect. It can be observed that the higher deflection is due to the increase of load parameters. In contrast, the deflection reduces with the increase in strain gradient parameter at a specific value of $\frac{\sqrt{\ell}}{a}$. As expected, this behavior causes by the enhancement in plate's stiffness.

Furthermore, the influences of porosity coefficient β on the load parameter versus deflection curves of porous S-FGM nanoplate at $\frac{\sqrt{\mu}}{a} = \frac{\sqrt{\ell}}{a} = 0.1$ are illustrated in Figs. 17 and 18 for two different patterns of porosity distribution. At a specific load parameter value, the increment value β generates the higher nonlinear deflection, the highest deflection value is found for $\beta = 0.7$. Also, through the comparison between Figs. 17 and 18, it can be seen that the nonlinear responses of Pattern A and Pattern B are similar under the influence of the porosity coefficient.

Finally, the effects of porosity distribution pattern on

deflection variation with load parameter of porous S-FGM nanoplate corresponding to different small size coefficients are illustrated in Figs. 19 and 20. It is observed that Pattern A generates lower nonlinear deflection than Pattern B under nonlocal effect and strain gradient effect at a specific value of load parameter. It is also known that the influence of the small size parameter on the difference between Pattern A and Pattern B is insignificant.

6. Conclusions

The size-dependent numerical approach based on the nonlocal strain gradient elasticity theory and IGA was established to explore the linear and nonlinear bending responses of porous S-FGM nanoplate. The Von-Kármán strain assumption and the Reissner-Mindlin plate theory are utilized to establish the nonlinear global equilibrium equations that are solved by using the Newton-Raphson procedure. The influences of porosity, power indexes, aspect ratios, nonlocal and strain gradient parameters on the linear and nonlinear porous S-FGM nanoplate are investigated. The symmetric and asymmetric porosity distribution across the plate's thickness is considered.

Acknowledgement

This research is funded by Vietnam National Foundation for Science and Technology Development (NAFOSTED) under grant number 107.02-2020.27.

References

Ahmed, R.A., Al-Maliki, A.F. and Faleh, N.M. (2020), "Dynamic characteristics of multi-phase crystalline porous shells with using strain gradient elasticity", *Adv. Nano Res.*, **8**(2), 157-167. https://doi.org/10.12989/anr.2020.8.2.157.

Ansari, R. and Norouzzadeh, A. (2016), "Nonlocal and surface effects on the buckling behavior of functionally graded nanoplates: An isogeometric analysis", *Physica E*, **84**, 84-97. https://doi.org/10.1016/j.physe.2016.05.036.

Ansari, R., Torabi, J. and Norouzzadeh, A. (2018), "Bending analysis of embedded nanoplates based on the integral formulation of Eringen's nonlocal theory using the finite element method", *Physica B*, **534**, 90-97. https://doi.org/10.1016/j.physb.2018.01.025.

Arefi, M., Kiani, M. and Zamani, M.H. (2018), "Nonlocal strain gradient theory for the magneto-electro-elastic vibration response of a porous FG-core sandwich nanoplate with piezomagnetic face sheets resting on an elastic foundation", *J. Sandw. Struct. Mater.*, **22**(7), 2157-2185. https://doi.org/10.1177/1099636218795378.

Abouelregal, A.E., Mohammad-Sedighi, H., Faghidian, S.A. and Shirazi, A.H. (2021), "Temperature-dependent physical characteristics of the rotating nonlocal nanobeams subject to a varying heat source and a dynamic load", *Facta Universitatis Mech. Eng.*, **19**(4), 633-656. https://doi.org/10.22190/FUME201222024A.

Abdulrazzaq, M.A., Fenjan, R.M., Ahmed, R.A. and Faleh, N.M. (2020), "Thermal buckling of nonlocal clamped exponentially graded plate according to a secant function based refined theory", *Steel Compos. Struct.*, **35**(1), 147-57. http://doi.org/10.12989/scs.2020.35.1.147.

Babu, B. and Patel, B.P. (2019), "A new computationally efficient finite element formulation for nanoplates using second-order strain gradient Kirchhoff's plate theory", *Compos. Part B Eng.*, **168**, 302-311. https://doi.org/10.1016/j.compositesb.2018.12.066.

Chen, D., Feng, K. and Zheng, S. (2019), "Flapwise vibration analysis of rotating composite laminated Timoshenko microbeams with geometric imperfection based on a re-modified couple stress theory and isogeometric analysis", *Eur. J. Mech. A Solids*, **76**, 25-35. https://doi.org/10.1016/j.euromechsol.2019.03.002.

Chung, Y.L. and Chi, S. (2001), "The residual stress of functionally graded materials", *J. Chin. Inst. Civil Hydraulic Eng.*, **13**, 1-9.

Chai, Q. and Wang, Y.Q. (2022), "Traveling wave vibration of graphene platelet reinforced porous joined conical-cylindrical shells in a spinning motion", *Eng. Struct.*, **252**, 113718. https://doi.org/10.1016/j.engstruct.2021.113718.

Daikh, A.A., Houari, M.S.A. and Eltaher, M.A. (2021), "A novel nonlocal strain gradient Quasi-3D bending analysis of sigmoid functionally graded sandwich nanoplates", *Compos. Struct.*, **262**, 113347. https://doi.org/10.1016/j.compstruct.2020.113347.

Ebrahimi, F. and Barati, M.R. (2019), "Dynamic modeling of embedded nanoplate systems incorporating flexoelectricity and surface effects", *Microsyst. Technol.*, **25**(1), 175-187. https://doi.org/10.1007/s00542-018-3946-7.

Ebrahimi, F. and Seyfi, A. (2020). "Studying propagation of wave in metal foam cylindrical shells with graded porosities resting on variable elastic substrate", *Eng. Comput.*, 1-17. https://doi.org/10.1007/s00366-020-01069-w.

Ebrahimi, F., Jafari, A. and Selvamani, R. (2020), "Thermal buckling analysis of magneto-electro-elastic porous FG beam in thermal environment", *Adv. Nano Res.*, **8**(1), 83-94. https://doi.org/10.12989/anr.2020.8.1.083.

Ebrahimi, F., Dabbagh, A. and Taheri, M. (2021), "Vibration analysis of porous metal foam plates rested on viscoelastic substrate", *Eng. Comput.*, **37**(4), 3727-3739. https://doi.org/10.1007/s00366-020-01031-w.

Emadi, M., Nejad, M.Z., Ziaee, S. and Hadi, A. (2021b), "Buckling analysis of arbitrary two-directional functionally graded nano-plate based on nonlocal elasticity theory using generalized differential quadrature method", *Steel Compos. Struct.*, **39**(5), 565-581. https://doi.org/10.12989/scs.2021.39.4.419.

Eringen, A.C. and Edelen, D.G.B. (1972), "On nonlocal elasticity", *Int. J. Eng. Sci.*, **10**(3), 233-248. https://doi.org/10.1016/0020-7225(72)90039-0.

Eringen, A.C. (1972), "Nonlocal polar elastic continua", *Int. J. Eng. Sci.*, **10**(1), 1-16. https://doi.org/10.1016/0020-7225(72)90070-5.

Fan, F., Safaei, B. and Sahmani, S. (2021), "Buckling and postbuckling response of nonlocal strain gradient porous functionally graded micro/nano-plates via NURBS-based isogeometric analysis", *Thin Wall. Struct.*, **159**, 107231. https://doi.org/10.1016/j.tws.2020.107231.

Fattahi, A., Safaei, B. and Moaddab, E. (2019), "The application of nonlocal elasticity to determine vibrational behavior of FG nanoplates", *Steel Compos. Struct.*, **32**(2), 281-292. https://doi.org/10.12989/scs.2019.32.2.281.

Faleh, N.M., Fenjan, R.M. and Ahmed, R.A. (2018), "Dynamic analysis of graded small-scale shells with porosity distributions under transverse dynamic loads", *Eur. Phys. J. Plus*, **133**(9), 1-11. https://doi.org/10.1140/epjp/i2018-12152-5.

Fenjan, R.M., Moustafa, N.M. and Faleh, N.M. (2020a), "Scale-dependent thermal vibration analysis of FG beams having porosities based on DQM", *Adv. Nano Res*, **8**(4), 283-292.

https://doi.org/10.12989/anr.2020.8.4.283.

Fenjan, R.M., Ahmed, R.A., Faleh, N.M. and Hani, F.M. (2020b), "Static stability analysis of smart nonlocal thermo-piezo-magnetic plates via a quasi-3D formulation", *Smart Struct. Syst.*, **26**(1), 77-87. http://doi.org/10.12989/sss.2020.26.1.077.

Gain, A.K., Zhang, L. and Liu, W. (2015), "Microstructure and material properties of porous hydroxyapatite-zirconia nano-composites using polymethyl methacrylate powders", *Mater. Des.*, **67**, 136-144. https://doi.org/10.1016/j.matdes.2014.11.028.

He, L., Xu, J., Dekai, Z.H.O.U., Qinghai, Y.A.N.G. and Longqiu, L. (2018), "Potential application of functional micro-nano structures in petroleum", *Petrol. Explo. Develop.*, **45**(4), 745-753. https://doi.org/10.1016/S1876-3804(18)30077-6.

Hughes, T.J.R., Cottrell, J.A. and Bazilevs, Y. (2005), "Isogeometric analysis: CAD, finite elements, NURBS, exact geometry and mesh refinement", *Comput. Meth. Appl. Mech. Eng.*, **194**(39), 4135-4195. https://doi.org/10.1016/j.cma.2004.10.008.

Ishihara, M., Yoshida, T., Ootao, Y. and Kameo, Y. (2020), "Hygrothermoelasticity in a porous cylinder under nonlinear coupling between heat and moisture", *Struct. Eng. Mech.*, **75**(1), 59-69. https://doi.org/10.12989/sem.2020.75.1.059.

Jung, W.Y. and Han, S.C. (2013), "Analysis of sigmoid functionally graded material (S-FGM) nanoscale plates using the nonlocal elasticity theory", *Math. Probl. Eng.*, **2013**, 476131. https://doi.org/10.1155/2013/476131.

Jung, W.Y. and Han, S.C. (2015), "Static and eigenvalue problems of sigmoid functionally graded materials (S-FGM) micro-scale plates using the modified couple stress theory", *Appl. Math. Model.*, **39**(12), 3506-3524. https://doi.org/10.1016/j.apm.2014.11.056.

Kaci, A., Bakhti, K., Hebali, H. and Tounsi, A. (2013), "Mathematical solution for nonlinear cylindrical bending of sigmoid functionally graded plates", *J. Appl. Mech. Tech. Phys.*, **54**(1), 124-131. https://doi.org/10.1134/S002189441301015X.

Karami, B. and Karami, S. (2019), "Buckling analysis of nanoplate-type temperature-dependent heterogeneous materials", *Adv. Nano Res.*, **7**(1), 51-61. https://doi.org/10.12989/anr.2019.7.1.051.

Kim, W.J., Lee, W.H., Park, W.T. and Han, S.C. (2014), "Nonlocal elasticity effects on free vibration properties of sigmoid functionally graded material nano-scale plates", *J. Korea Acad. Ind. Coop. Soc.*, **15**(2), 1109-1117. https://doi.org/10.5762/KAIS.2014.15.2.1109.

Kim, J. and Reddy, J.N. (2015), "A general third-order theory of functionally graded plates with modified couple stress effect and the von Kármán nonlinearity: theory and finite element analysis", *Acta Mechanica*, **226**(9), 2973-2998. https://doi.org/10.1007/s00707-015-1370-y.

Koiter, W. (1964), "Couple-stresses in the theory of elasticity, I and II, Prec", *Roy. Netherlands Acad. Sci. B*, **67**, 0964.

Koizumi, M. (1993), "The concept of FGM", *Ceram. Transact.*, **34**, 3-10.

Koochi, A. and Goharimanesh, M. (2021), "Nonlinear oscillations of cnt nano-resonator based on nonlocal elasticity: The energy balance method", *Rep. Mech. Eng.*, **2**(1), 41-50. https://doi.org/10.31181/rme200102041g.

Khalaf, B.S., Fenjan, R.M. and Faleh, N.M. (2019), "Analyzing nonlinear mechanical-thermal buckling of imperfect micro-scale beam made of graded graphene reinforced composites", *Adv. Mater. Res.*, **8**(3), 219-235. https://doi.org/10.12989/amr.2019.8.3.219.

Lam, D.C., Yang, F., Chong, A.C.M., Wang, J. and Tong, P. (2003), "Experiments and theory in strain gradient elasticity", *J. Mech. Phys. Solids*, **51**(8), 1477-1508. https://doi.org/10.1016/S0022-5096(03)00053-X.

Lee, W.H., Han, S.C. and Park, W.T. (2012), "Nonlocal elasticity theory for bending and free vibration analysis of nano plates", *J. Korea Acad. Ind. Coop. Soc.*, **13**(7), 3207-3215. https://doi.org/10.5762/KAIS.2012.13.7.3207.

Lee, W.H., Han, S.C. and Park, W.T. (2015), "A refined higher order shear and normal deformation theory for E-, P-, and S-FGM plates on Pasternak elastic foundation", *Compos. Struct.*, **122**, 330-342. https://doi.org/10.1016/j.compstruct.2014.11.047.

Levy, S. and Chiarito, P.T. (1942), *Square Plate with Clamped Edges Under Normal Pressure Producing Large Deflections*, National Advisory Committee for Aeronautics, U.S. Government Printing Office, U.S.A.

Lim, C.W., Zhang, G. and Reddy, J.N. (2015), "A higher-order nonlocal elasticity and strain gradient theory and its applications in wave propagation", *J. Mech. Phys. Solids*, **78**, 298-313. https://doi.org/10.1016/j.jmps.2015.02.001.

Liu, S., Yu, T., Bui, T.Q. and Xia, S. (2020), "Size-dependent analysis of homogeneous and functionally graded microplates using IGA and a non-classical Kirchhoff plate theory", *Compos. Struct.*, **172**, 34-44. https://doi.org/10.1016/j.compstruct.2017.03.067.

Liu, H., Zhang, Q., Yang, X. and Ma, J. (2021), "Size-dependent vibration of laminated composite nanoplate with piezo-magnetic face sheets", *Eng. Comput.*, 1-17. https://doi.org/10.1007/s00366-021-01285-y.

Ma, L.H., Ke, L.L., Wang, Y.Z. and Wang, Y.S. (2018), "Wave propagation analysis of piezoelectric nanoplates based on the nonlocal theory", *Int. J. Struct. Stabil. Dynam.*, **18**(4), 1850060. https://doi.org/10.1142/S0219455418500608.

Mechab, I., Mechab, B., Benaissa, S., Serier, B. and Bouiadjra, B.B. (2016), "Free vibration analysis of FGM nanoplate with porosities resting on Winkler Pasternak elastic foundations based on two-variable refined plate theories", *J. Brazil. Soc. Mech. Sci. Eng.*, **38**(8), 2193-2211. https://doi.org/10.1007/s40430-015-0482-6.

Mindlin, R.D. (1963), "Microstructure in linear elasticity", Research Report No. AD0424156; Department of Civil Engineering and Engineering Mechanics, Columbia University of New York, New York, U.S.A.

Mindlin, R.D. and N. (1968), "Eshel, On first strain-gradient theories in linear elasticity", *Int. J. Solid. Struct.*, **4**(1), 109-124. https://doi.org/10.1016/0020-7683(68)90036-X.

Miyamoto, Y., Kaysser, W.A., Rabin, B.H., Kawasaki, A. and Ford, R.G. (2013), "Functionally graded materials: design, processing and applications", Springer Science & Business Media, **5**.

Mueller, E., Drašar, Č., Schilz, J. and Kaysser, W.A, (2003), "Functionally graded materials for sensor and energy applications", *Mater. Sci. Eng. A*, **362**(1-2), 17-39. https://doi.org/10.1016/S0921-5093(03)00581-1.

Moory-Shirbani, M., Sedighi, H.M., Ouakad, H.M. and Najar, F, (2018), "Experimental and mathematical analysis of a piezoelectrically actuated multilayered imperfect microbeam subjected to applied electric potential", *Compos. Struct.*, **184**, 950-960. https://doi.org/10.1016/j.compstruct.2017.10.062.

Natarajan, S., Chakraborty, S., Thangavel, M., Bordas, S. and Rabczuk, T. (2012), "Size-dependent free flexural vibration behavior of functionally graded nanoplates", *Comput. Mater. Sci.*, **65**, 74-80. https://doi.org/10.1016/j.commatsci.2012.06.031.

Nguyen, N.T., Hui, D., Lee, J. and Nguyen-Xuan, H. (2015), "An efficient computational approach for size-dependent analysis of functionally graded nanoplates", *Comput. Meth. Appl. Mech. Eng.*, **297**, 191-218. https://doi.org/10.1016/j.cma.2015.07.021.

Norouzzadeh, A., Ansari, R. and Rouhi, H. (2019), "Nonlinear bending analysis of nanobeams based on the nonlocal strain gradient model using an isogeometric finite element approach", *Iran. J. Sci. Technol. Transact. Civil Eng.*, **43**(1), 533-547. https://doi.org/10.1007/s40996-018-0184-2.

Ouakad, H.M., Valipour, A., Żur, K.K., Sedighi, H.M. and Reddy, J.N. (2020), "On the nonlinear vibration and static deflection problems of actuated hybrid nanotubes based on the stress-driven nonlocal integral elasticity", *Mech. Mater.*, **148**, 103532. https://doi.org/10.1016/j.mechmat.2020.103532.

Pompe, W., Worch, H., Epple, M., Friess, W., Gelinsky, M., Greil, P., Hempel, U., Scharnweber, D. and Schulte, K.J.M.S. (2003), "Functionally graded materials for biomedical applications", *Mater. Sci. Eng. A*, **362**(1-2), 40-60. https://doi.org/10.1016/S0921-5093(03)00580-X.

Reddy, J.N. (2004), "Mechanics of laminated composite plates and shells theory and analysis", CRC Press, New York, U.S.A.

Samaniego, E., Anitescu, C., Goswami, S., Nguyen-Thanh, V.M., Guo, H., Hamdia, K., Zhuang, X. and Rabczuk, T. (2020), "An energy approach to the solution of partial differential equations in computational mechanics via machine learning: Concepts, implementation and applications", *Comput. Method. Appl. Mech. Eng.*, **362**, 112790. https://doi.org/10.1016/j.cma.2019.112790.

Sahmani, S., Fattahi, A.M. and Ahmed, N.A. (2020), "Analytical treatment on the nonlocal strain gradient vibrational response of postbuckled functionally graded porous micro-/nanoplates reinforced with GPL", *Eng. Comput.*, **36**(4), 1559-1578. https://doi.org/10.1007/s00366-019-00782-5.

Shariati, A., Mohammad-Sedighi, H., Żur, K.K., Habibi, M. and Safa, M. (2020a), "Stability and dynamics of viscoelastic moving rayleigh beams with an asymmetrical distribution of material parameters", *Symmetry*, **12**(4), 586. https://doi.org/10.3390/sym12040586.

Shariati, A., Ebrahimi, F., Karimiasl, M., Vinyas, M. and Toghroli, A. (2020b), "On transient hygrothermal vibration of embedded viscoelastic flexoelectric/piezoelectric nanobeams under magnetic loading", *Adv. Nano Res.*, **8**(1), 49-58. https://doi.org/10.12989/anr.2020.8.1.049.

Sedighi, H.M., Ouakad, H.M., Dimitri, R. and Tornabene, F. (2020), "Stress-driven nonlocal elasticity for the instability analysis of fluid-conveying C-BN hybrid-nanotube in a magneto-thermal environment", *Phys. Scripta*, **95**(6), 065204. https://doi.org/10.1088/1402-4896/ab793f.

Sedighi, H.M. and Malikan, M. (2020), "Stress-driven nonlocal elasticity for nonlinear vibration characteristics of carbon/boron-nitride hetero-nanotube subject to magneto-thermal environment", *Phys. Scripta*, **95**(5), 055218. https://doi.org/10.1088/1402-4896/ab7a38.

Singh, P.P. and Azam, M.S. (2020), "Free vibration and buckling analysis of elastically supported transversely inhomogeneous functionally graded nanoplate in thermal environment using Rayleigh–Ritz method", *J. Vib. Control*, **27**(23-24), 2835-2847. https://doi.org/10.1177/1077546320966932.

Singh, S.J. and Harsha, S.P. (2019), "Nonlinear dynamic analysis of sandwich S-FGM plate resting on pasternak foundation under thermal environment", *Eur. J. Mech. A Solids*, **76**, 155-179. https://doi.org/10.1016/j.euromechsol.2019.04.005.

Singh, S.J. and Harsha, S.P. (2020), "Analysis of porosity effect on free vibration and buckling responses for sandwich sigmoid function based functionally graded material plate resting on Pasternak foundation using Galerkin Vlasov's method", *J. Sandw. Struct. Mater.*, **23**(5), 1717-1760. https://doi.org/10.1177/1099636220904340.

Sobhy, M.A. (2015), "Comprehensive study on FGM nanoplates embedded in an elastic medium", *Compos. Struct.*, **134**, 966-980. https://doi.org/10.1016/j.compstruct.2015.08.102.

Thai, C.H., Ferreira, A.J.M. and Phung-Van, P. (2020), "A nonlocal strain gradient isogeometric model for free vibration and bending analyses of functionally graded plates", *Compos. Struct.*, **251**, 112634. https://doi.org/10.1016/j.compstruct.2020.112634.

Thai, T.Q., Zhuang, X. and Rabczuk, T. (2021), "A nonlinear geometric couple stress based strain gradient Kirchhoff–Love shell formulation for microscale thin-wall structures", *Int. J. Mech. Sci.*, **196**, 106272. https://doi.org/10.1016/j.ijmecsci.2021.106272.

Rabczuk, T., Ren, H., Zhuang, X. (2019), "A nonlocal operator method for partial differential equations with application to electromagnetic waveguide problem", *Comput. Mater. Continua*, **59**(1), 31-55. https://doi.org/10.32604/cmc.2019.04567.

Thang, P.T., Nguyen-Thoi, T. and Lee, J. (2016), "Closed-form expression for nonlinear analysis of imperfect sigmoid-FGM plates with variable thickness resting on elastic medium", *Compos. Struct.*, **143**, 143-150. https://doi.org/10.1016/j.compstruct.2016.02.002.

Thanh, C.L., Tran, L.V., Vu-Huu, T., Nguyen-Xuan, H. and Abdel-Wahab, M. (2019a), "Size-dependent nonlinear analysis and damping responses of FG-CNTRC micro-plates", *Comput. Methods Appl. Mech. Eng.*, **353**, 253-276. https://doi.org/10.1016/j.cma.2019.05.002.

Thanh, C.L., Tran, L.V., Bui, T.Q., Nguyen, H.X. and Abdel-Wahab, M. (2019b), "Isogeometric analysis for size-dependent nonlinear thermal stability of porous FG microplates", *Compos. Struct.*, **221**, 110838. https://doi.org/10.1016/j.compstruct.2019.04.010.

Thanh, C.L., Ferreira, A. and Wahab, M.A. (2019c), "A refined size-dependent couple stress theory for laminated composite micro-plates using isogeometric analysis", *Thin Wall. Struct.*, **145**, 106427. https://doi.org/10.1016/j.cma.2019.05.002.

Thanh, C. L., Nguyen, T.N., Vu, T.H., Khatir, S. and Wahab, M.A. (2020), "A geometrically nonlinear size-dependent hypothesis for porous functionally graded micro-plate", *Eng. Comput.*, 1-12. https://doi.org/10.1007/s00366-020-01154-0.

Thanh, C.L., Nguyen, K.D., Lee, J., Rabczuk, T. and Nguyen-Xuan, H. (2021), "A 3D nano scale IGA for free vibration and buckling analyses of multi-directional FGM nanoshells", *Nanotechnology*, **33**(6), 065703. https://doi.org/10.1088/1361-6528/ac32f9.

Toupin, R. (1962), "Elastic materials with couple-stresses", *Arch. Ration. Mech. An.*, **11**(1), 385-414.

Teng, M.W. and Wang, Y.Q. (2021), "Nonlinear forced vibration of simply supported functionally graded porous nanocomposite thin plates reinforced with graphene platelets", *Thin Wall. Struct.*, **164**, 107799. https://doi.org/10.1016/j.tws.2021.107799.

Van Vinh, P. (2022), "Nonlocal free vibration characteristics of power-law and sigmoid functionally graded nanoplates considering variable nonlocal parameter", *Physica E*, **135**, 114951. https://doi.org/10.1016/j.physe.2021.114951.

Wang, Y.Q. and Zu, J.W. (2017a), "Vibration behaviors of functionally graded rectangular plates with porosities and moving in thermal environment", *Aerosp. Sci. Technol.*, **69**, 550-562. https://doi.org/10.1016/j.ast.2017.07.023.

Wang, Y.Q. and Zu, J.W. (2017b), "Large-amplitude vibration of sigmoid functionally graded thin plates with porosities", *Thin Wall. Struct.*, **119**, 911-924. https://doi.org/10.1016/j.tws.2017.08.012.

Wang, Y.Q. (2018), "Electro-mechanical vibration analysis of functionally graded piezoelectric porous plates in the translation state", *Acta Astronautica*, **143**, 263-271. https://doi.org/10.1016/j.actaastro.2017.12.004.

Wang, Y.Q., Ye, C. and Zu, J.W. (2019), "Nonlinear vibration of metal foam cylindrical shells reinforced with graphene platelets", *Aerosp. Sci. Technol.*, **85**, 359-370. https://doi.org/10.1016/j.ast.2018.12.022.

Yang, F.A.C.M., Chong, A.C.M., Lam, D.C.C. and Tong, P. (2002), "Couple stress based strain gradient theory for elasticity", *Int. J. Solids Struct.*, **39**(10), 2731-2743. https://doi.org/10.1016/S0020-7683(02)00152-X.

Ye, C. and Wang, Y.Q. (2021), "Nonlinear forced vibration of functionally graded graphene platelet-reinforced metal foam cylindrical shells: Internal resonances", *Nonlinear Dynam*., **104**(3), 2051-2069. https://doi.org/10.1007/s11071-021-06401-7.

Xiang, T., Hou, J., Xie, H., Liu, X., Gong, T. and Zhou, S. (2020), "Biomimetic micro/nano structures for biomedical applications", *Nano Today*, **35**, 100980. https://doi.org/10.1016/j.nantod.2020.100980.

Xu, H., Wang, Y.Q. and Zhang, Y. (2021), "Free vibration of functionally graded graphene platelet-reinforced porous beams with spinning movement via differential transformation method", *Arch. Appl. Mech*., **91**(12), 4817-4834. https://doi.org/10.1007/s00419-021-02036-7.

Zhang, Z., Li, H.N. and Yao, L.Q. (2021), "Vibration analysis of flexoelectric nanoplates based on nonlocal theory", *Proceedings of the 2020 15th Symposium on Piezoelectrcity, Acoustic Waves and Device Applications*, Zhengzhou, Henan Province, China, April.

Zhuang, X., Guo, H., Alajlan, N., Zhu, H. and Rabczuk, T. (2021), "Deep autoencoder based energy method for the bending, vibration, and buckling analysis of Kirchhoff plates with transfer learning", *Eur. J. Mech. A Solids*, **87**, 104225. https://doi.org/10.1016/j.euromechsol.2021.104225.

Zhou, C., Zhang, Z., Zhang, J., Fang, Y. and Tahouneh, V. (2020), "Vibration analysis of FG porous rectangular plates reinforced by graphene platelets", *Steel Compos. Struct*., **34**(2), 215-226. https://doi.org/10.12989/scs.2020.34.2.215.

Yan, K., Zhang, Y., Cai, H. and Tahouneh, V. (2020), "Vibrational characteristic of FG porous conical shells using Donnell's shell theory", *Steel Compos. Struct*., **35**(2), 249-260. https://doi.org/10.12989/scs.2020.35.2.249.

She, G.L., Liu, H.B. and Karami, B. (2020), "On resonance behavior of porous FG curved nanobeams", *Steel Compos. Struct*, **36**(2), 179-186. https://doi.org/10.12989/scs.2020.36.2.179.

Si, H., Shen, D., Xia, J. and Tahouneh, V. (2020), "Vibration behavior of functionally graded sandwich beam with porous core and nanocomposite layers", *Steel Compos. Struct*,, **36**(1), 1-16. https://doi.org/10.12989/scs.2020.36.1.001.

Khaniki, H.B., Ghayesh, M.H., Hussain, S. and Amabili, M. (2020), "Porosity, mass and geometric imperfection sensitivity in coupled vibration characteristics of CNT-strengthened beams with different boundary conditions", *Eng. Comput*., 1-27. https://doi.org/10.1007/s00366-020-01208-3.

Khazaei, P. and Mohammadimehr, M. (2020), "Size dependent effect on deflection and buckling analyses of porous nano-composite plate based on nonlocal strain gradient theory", *Struct. Eng. Mech*., **76**(1), 27-56. https://doi.org/10.12989/sem.2020.76.1.027.

Shan, W., Deng, Z., Zhong, H., Mo, H., Han, Z., Yang, Z., Xiang, C., Li, S. and Liu, P. (2020), "Propagation characteristics of longitudinal wave, shear wave and bending wave in porous circular nanoplates", *Struct. Eng. Mech*., **76**(4), 551-559. https://doi.org/10.12989/sem.2020.76.4.551.

Nomenclature

h, a	The thickness and width of plate
E_{m}, E_{c}	The Young's modulus of metal and Ceramic
ν_m, ν_c	The Poisson ratio of metal and Ceramic
n, β	Power index and porosity coefficient
$\boldsymbol{\tau}$	The total stress tensor
$\boldsymbol{\tau}^0$, $\boldsymbol{\tau}^1$	The classical nonlocal stress and the higher-order stress tensors
μ, ℓ	The nonlocal parameter and gradient parameter.
α_0	The nonlocal attenuation function
α_1	The nonlocal effect corresponding
$\boldsymbol{\sigma}$	The local stress tensor
ρ	The mass density
$\ddot{\boldsymbol{u}}$	The accelerator component
$\mathbf{b}$	The body forces
u, v, w	The displacement of a point in plate domain
u_0, v_0, w_0	The displacements of the middle plane
β_x β_y	The rotations
$\varepsilon_x, \varepsilon_y, \gamma_{xy}, \gamma_{xz}, \gamma_{yz}$	The stress components
A	The number of control points
K_L, K_{NL}	The general linear and nonlinear stiffness matrix
f	The general forces vector
x, y, z	x, y, z-coodinate
K_g	The geometric stiffness matrix